On the acoustic radiation efficiency of local resonance based stop band materials

Claus C. Claeys, Paul Sas, Wim Desmet

Department of Mechanical Engineering,
KU Leuven
Celestijnenlaan 300B, B-3001 Heverlee (Leuven), Belgium

Abstract

The application of materials with stop bands is emerging as a novel way of creating meta-materials with good vibrational behaviour. The acoustic radiation efficiency in these stop band zones is often not investigated. This paper formulates an uncoupled vibro-acoustic unit cell model of a plate with local resonant stop band behaviour, based on the addition of a grid of tuned resonators. The results are compared with a vibro-acoustic coupled model for a finite equivalent of the infinite structure. It is shown that the beneficial vibration reduction that is achieved in a stop band can be acoustically reduced or enhanced by the change in radiation efficiency of the structure. When care is taken in the design of the stop band, a stop band material with good vibro-acoustic behaviour can be achieved.

Keywords: tuned resonators, stop bands, vibro-acoustic insulation

1. Introduction

Periodic structures, such as honeycomb core panels, combine good mechanical properties (strength and stiffness) with a low mass, making them attractive for application in the transportation and machine design sector. However, the high stiffness to mass ratio of these lightweight structures may result in unsatisfactory dynamic behaviour in that it may impair the panels ability to reduce noise and vibration levels.

*e-mail: claus.claeys@mech.kuleuven.be

In recent literature, the application of stop bands emerges as a novel method with good prospects for improving the NVH behaviour of structures [1, 2]. Stop bands, i.e. zones with no free wave propagation in a certain frequency range of interest, are achieved through mainly two approaches [3]: Bragg scattering or local resonances. In a previous work, the authors concluded that resonance based stopbands are more promising to obtain low-frequency stopbands with strong vibrational attenuation [4]. These stopbands depend on the addition of local resonators and the resonance frequency determines in which frequency zone attenuation is achieved [1].

This paper investigates the potential of local resonance stop bands in periodic structures for acoustic applications. Acoustic radiation results from the vibro-acoustic coupling between structural and acoustic waves. Since local resonance based stop bands drastically change the structural wave propagation, it is expected that the vibro-acoustic coupling can be strongly affected by the presence of stop bands. In the past Mead already investigated the acoustic behaviour of periodic engineering structures such as stiffened beams [5] and plates [6]. In recent literature, stop bands for use in acoustic applications are investigated [7, 8]. However, additional attention should be paid to the effect of resonance based stop bands on the radiation efficiency of propagating wave with frequencies close to the stop band region. This paper shows that coincidence is a determining factor for the acoustic radiation of structures in the stop band region.

This paper investigates local resonance based stop bands based on the addition of a grid of tuned resonators (TRs). This stop band mechanism is easy to grasp, allows straightforward manipulation and results in a clear split in dispersion curves, characteristic for resonance based stop bands. Addition of tuned resonators on a plate, mostly with random positions, is a thoroughly investigated academic example, both on a vibrational level [9] as well as on an acoustic level [10]. This paper extends previous work in that it relates these finding to the novel field of resonance based stop bands, resulting in guidelines for stop band design.

The paper starts with showing the effect of local resonance based stop bands on the radiation efficiency for infinite panels. Subsequently, a finite plate with a grid of damped TRs serves as a test case to assess the effect of stop bands on the acoustic radiation efficiency of finite panels. A section is devoted to the transition from infinite to finite panels, followed by a section where the

acoustic radiation efficiency of finite panels is evaluated and the findings from the first section are confirmed. The paper ends with conclusions and some guidelines regarding the acoustic radiation efficiency of stop bands.

2. Modelling the acoustic radiation of infinite periodic structures

This section briefly discusses the structural part of infinite periodic structure modelling and describes the evaluation of the structural-acoustic coupling.

2.1. Structural model

This paper considers periodic panels which allows a simplification of the modelling process; a unit cell characterizes the behaviour of the entire structure. Based on the model of the unit cell, the dispersion curves for an infinite structure can be calculated. These dispersion curves indicate for which frequencies waves will propagate without attenuation. Consequently it can be derived in which frequency ranges only attenuated wave propagation is possible, meaning that a stop band is found. This procedure is well documented in literature [11, 12, 13] and the interested reader is referred to those works.

To mimic the behaviour of the unit cell as if it were embedded in an infinite structure, the Bloch-Floquet boundary conditions are applied. These conditions link the degrees of freedom on the boundary of the unit cell as a function of the wave vector $\vec{k}$. Application of the Bloch-Floquet boundary conditions on a Finite Element Model (FEM) of the unit cell reduces the equations of motion for steady-state harmonic response [14]. This reduced form becomes a linear eigenvalue problem for free wave propagation in undamped structures, meaning that the wave vector $\vec{k}$ has only imaginary components. The frequencies of free wave propagation for every imaginary wave vector can thus be retrieved [14].

By solving the linear eigenvalue problem for all possible wave vectors the dispersion surfaces are obtained. Since the analyzed structure is periodic, also the solutions in the wave domain will be periodic. The smallest area in the wave space that contains all information is called the irreducible Brillouin zone [11, 12]. For computational efficiency reasons, the wave vectors are

restricted to the contours of this zone to explore stop bands, since the band extrema almost always occur along the contour of this zone [12, 15].

This focuses on symmetric square unit cells. For these kinds of unit cells, the irreducible Brillouin zone is triangular with as corner points the wave vectors which result in phase shifts $(0, 0)$, $(0, \pi)$ and (π, π) across the (x, y)-direction of the unit cell [13]. These corner points will be marked with the notation O, A and B. When investigating the irreducible Brillouin contour, only the edges of the triangle with corner points O,A,B,O $\mapsto$ $(0, 0), (0, \pi), (\pi, \pi), (0, 0)$ needs to be investigated.

Since the wave vector in this context is characterised by the phase shift across the unit cell, the wave vector is often written as the propagation vector

$$\boldsymbol{\epsilon} = (k_x L_x, k_y L_y) \tag{1}$$

with k_x, k_y the wave vector components and L_x, L_y the length of the unit cell in x- resp, y-direction.

Only the dispersion curves linked to the out-of-plane motion of the plate are examined. The in-plane modes of the plate are decoupled from the out-of-plane modes for flat plates and can be omitted from a vibro-acoustic point of view.

2.2. Acoustic model

The dispersion equation governs the relation between wave propagation and wave speed in an acoustic medium, when considering an ideally compressible, linear fluid and neglecting viscosity and thermal effects [16];

$$c_{ac} = 2\pi f / k_{ac}. \tag{2}$$

where k_{ac} is the magnitude of the wave vector in the acoustic medium, f is the frequency of propagation and c_{ac} is the wave speed in the acoustic medium.

The coupling between flexural and acoustic waves determines the efficiency of the transmission of flexural waves into an acoustic domain. The acoustic wave radiated from the structure can

be seen as having an in-plane ($k_{\_}$) component in the interface plane between the structure and the acoustic domain and an out-of-plane component ($k_{\perp}$) into the acoustic domain. The freely propagating flexural structural wave with magnitude $k_{str} = \|\vec{\mathbf{k}}_{str}\|$ lies in the interface plane and acts as a boundary condition for the acoustic wave; the magnitude of the in-plane component of the acoustic wave will equal the magnitude of the structural wave ($k_{\_} = k_{str}$). The structure-acoustic coupling is efficient if the magnitude of the acoustic wave $k_{ac} = \sqrt{k_{\perp}^2 + k_{\_}^2}$ equals or exceeds the magnitude of the structural wave [16]. This statement combined with eq. (2) can be expressed as:

$$\Rightarrow k_{\perp} = \sqrt{(2\pi f/c_{ac})^2 - k_{str}^2}, \tag{3}$$

where $k_{\perp}$ needs to be real for efficient acoustic radiation. The frequency for which $k_{\perp} = 0$ is the most efficient frequency of acoustic radiation and is called the coincidence frequency.

2.3. Acoustic radiation on Brillouin contour

Each point on the dispersion curve from the structural model, links a certain structural wave vector with a frequency of free wave propagation. These can be used in eq. (3) to assess the efficiency of acoustic radiation. Combination of both allows to indicate which points on the irreducible Brillouin contour will have an efficient vibro-acoustic coupling.

Care should be taken in translating the wave vectors on the irreducible Brillouin contour to in-plane components ($k_{\_}$) of the acoustic wave; since due to the periodicity in the wave domain, not only the structural wave with wave vector (ϵ_x, ϵ_y) will be a solution of the unit cell analysis, but also all structural waves with wave vector $(2n\pi \pm \epsilon_x, 2m\pi \pm \epsilon_y)$ with $n, m \in \mathbb{Z}$. To assure that the correct wave number was chosen for evaluating the acoustic coupling, a spatial Fourier Transform of the displacement field was used to obtain the correct structural wave number.

In this paper coincidence is only investigated in the first Brillouin zone and for acoustic wave vectors in this fundamental interval. This is equivalent to stating that coincidence is only investigated for acoustic wavelengths larger than half the unit cell length. For smaller acoustic wavelengths, at higher frequencies, higher order Brillouin zones should be investigated as well. Since this paper concerns low-frequency stop bands for acoustic applications, only inspection

of this lower frequency range is necessary. From the examples it can be seen that coincidence always occurs in this frequency range.

3. Application on an infinite steel plate

An infinite steel plate (Table 1) serves as a test case to investigate the effect of stop bands on the vibro-acoustic coupling. To introduce stop bands, TRs are added on a periodic grid. The unit cell (Fig. 1) is symmetrical and square. The mass (m) of the TR is 20% of the mass of the plate in the unit cell and the stiffness (k) of the resonator is changed throughout the examples.

Table 1: Material characteristics and cross-sectional dimension of the infinite plate used.

Young's modulus (E)	Density (ρ)	Poisson's ratio (ν)	Thickness (t)	Cell length (L)
210 GPa	7800 $\frac{\text{kg}}{\text{m}^3}$	0.3	5 mm	50 mm

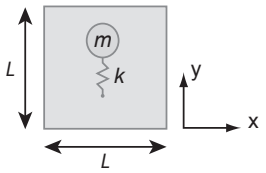

Figure 1: Square unit cell of an infinite plate with a grid of periodic TRs.

The Kirchhoff-plate-theory expresses the dispersion relationship between frequency and wave vector for bending waves in an infinite plate as:

$$f = \frac{1}{2\pi k^2}\sqrt{\frac{t^2 E}{12(1-\nu^2)\rho}}. \tag{4}$$

From Table 1 and eqs. (3) and (4) it can be derived that the coincidence frequency for the considered plate equals 2343Hz. To assess the effect of stop bands on the radiation efficiency, three different cases are investigated; plates with TR resonances of 1171, 2343 and 3946 Hz, corresponding to resp. 50, 100 and 160% of the coincidence frequency of the steel plate without TRs. Previous work [4] shows that the limit frequency for stop bands can be derived from eq. (4) with $k = \pi/L$. This equals 4930 Hz for the considered unit cell and plate characteristics: each TR

configuration considered, will have a stop band in the region of the TR resonance.

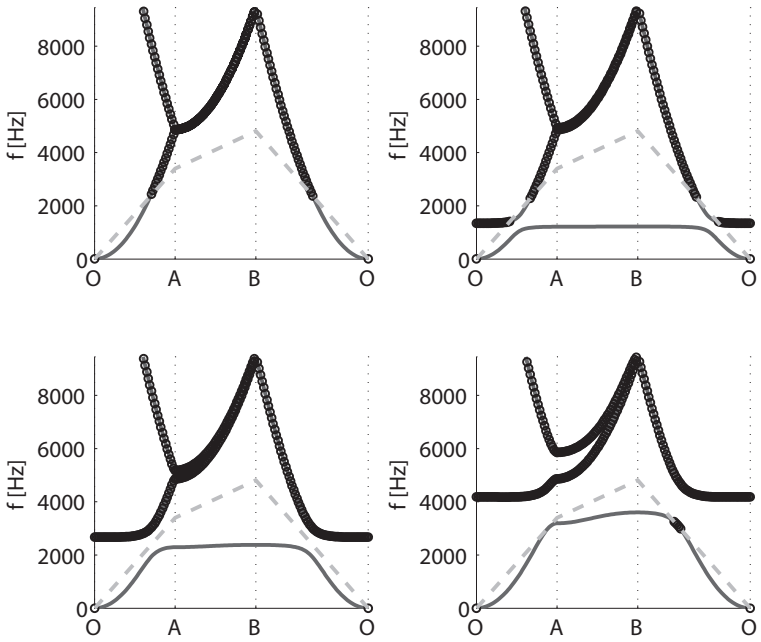

Figure 2: Dispersion curves along the irreducible Brillouin Contour (—) O,A,B,O $\mapsto (0,0),(0,\pi),(\pi,\pi),(0,0)$, see section 2.1, of the structure (—) , the structural free propagating waves that will radiate efficiently (∘) and the dispersion curve of air (- - -). Only coincidence with acoustic waves with wavelengths larger than twice the unit cell length are investigated. From left to right and bottom to top: an infinite steel plate (Table 1) and the same plate with a grid of TRs; tuned at resp. 1171, 2343 and 3946 Hz.

Figure 2 compares the dispersion diagrams for the different cases and indicates the zones of efficient acoustic radiation. When no TRs are present efficient radiation starts at 2343 Hz, as predicted. If the TR resonance equals half the coincidence frequency (1171 Hz) an additional zone of efficient radiation is created for frequencies just above the stop band. This new zone of efficient radiation leads to a second coincidence frequency; at the highest frequency of this zone, the acoustic wave vector matches the structural wave vector.

When the TRs are tuned to the coincidence frequency (2343 Hz), the efficient radiation starts

at higher frequencies and no additional zone of efficient radiation is created. If the TR resonance is high enough with respect to the coincidence frequency, e.g. 160% or 3946 Hz, there appear again two separate zones of efficient radiation. The total length of the efficient zone is smaller than for the original system; however, for this configuration, two new coincidence frequencies are created.

Table 2 compares the different test cases in terms of stop band width and zones of efficient acoustic radiation. For the sake of comparison also an equivalent steel plate, without TRs but increased mass to match the TR mass, is considered. This plate, with unchanged stiffness but a 20% increase in density, has a coincidence frequency of 2567 Hz.

Table 2: Comparison of stop band widths and zones of efficient acoustic coupling for a steel plate, a steel plate with a grid of TRs tuned at f_{res} and a steel plate with a mass equal to the one of the plate with a grid of TRs.

Case	Stop Band	Efficient radiation
original plate	-	> 2343 Hz
equivalent plate	-	> 2567 Hz
f_{res} =1171 Hz	1223-1349 Hz	1349-1409 Hz, > 2250 Hz
f_{res} =2343 Hz	2379-2671 Hz	> 2672 Hz
f_{res} =3514 Hz	3601-4178 Hz	2981-3254 Hz, > 4178 Hz

Since the evaluation of radiation efficiency for infinite structures is based on freely propagating wave vectors, the radiation efficiency in the stop band zone can't be evaluated. In the section where the acoustic radiation of a finite plate is investigated, the radiation efficiency in the stop band will be evaluated.

4. Transition from infinite to finite plates

This section describes by means of an example the link between dispersion diagrams of infinite structures and the modal behaviour of equivalent finite structures. Next this example is

used to gain more insight into the characteristic split in dispersion surfaces of local resonance based stop band materials.

4.1. Sampling on dispersion surface

The dispersion surface of infinite periodic structures allows predicting eigenvalues of the finite counterparts of those structures [17]. The dispersion surface of the infinite structures can be calculated based on the infinite periodic structure model. The reduced eigenvalue problem is solved for a grid of wave vectors with both ϵ_x and ϵ_y ranging from 0 to π in order to cover the entire range of expected eigenvalues.

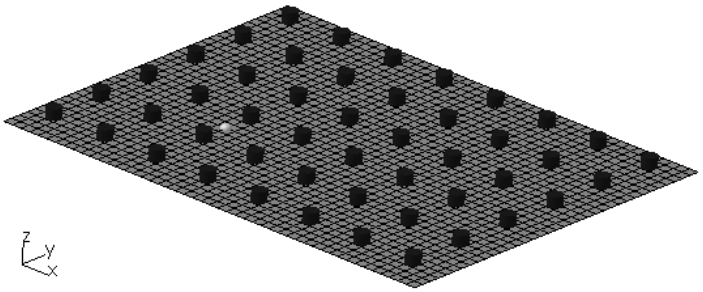

Figure 3: Finite plate (0.4 m by 0.3 m with TRs (dark cylinders). The light sphere indicates the excitation point for the acoustic analysis.

In this paper a finite plate is derived by repeating the unit cell 8x6 times so that a plate of 0.4 m by 0.3 m is obtained (Fig. 3). The plate is simply supported along its boundaries. According to Mead and Parthan [17] the natural frequencies for finite periodic plates with N_x symmetrical elements in the x-direction, N_y in the y-direction and supported edges, can be found by sampling the dispersion surfaces on the points corresponding to the wave vectors ($m\pi/N_x$,$n\pi/N_y$) with $m = 1, 2, ..., N_x$ and $n = 1, 2, ..., N_y$.

The correspondence between the finite and infinite structure is verified by displaying the eigenfrequencies of the finite structure together with the dispersion surfaces of the infinite structure. Visual inspection of the mode shape and counting the number of half wave lengths fitting in x- and y-direction, allows combining each eigenfrequency with a certain phase-shift (ϵ_x, ϵ_y) across the unit cell. The corresponding phase shift per cell in x- and y-direction for the infinite

structure is calculated as:

$$(\epsilon_x, \epsilon_y) = (\frac{\pi n_x L_{UC,x}}{L_x}, \frac{\pi n_y L_{UC,y}}{L_y}) \tag{5}$$

with $L_{UC,x}$, $L_{UC,y}$ the length of the unit cell in x- resp, y-direction, L_x, L_y the length of the plate in x- resp, y-direction and n_x, n_y the number of half wave lengths in x- resp. y-direction for the considered eigenmode.

The eigenfrequencies below 5000Hz are calculated with a Nastran solver for both a plate without TRs as well as a plate with TRs tuned at half the coincidence frequency. The FEM of the finite plate with TRs consists of 1861 nodes, 1728 linear Quad4 elements, 48 Bush elements and 48 Point Mass elements. For the plate without TRs, the Bush and Point Mass elements were removed.

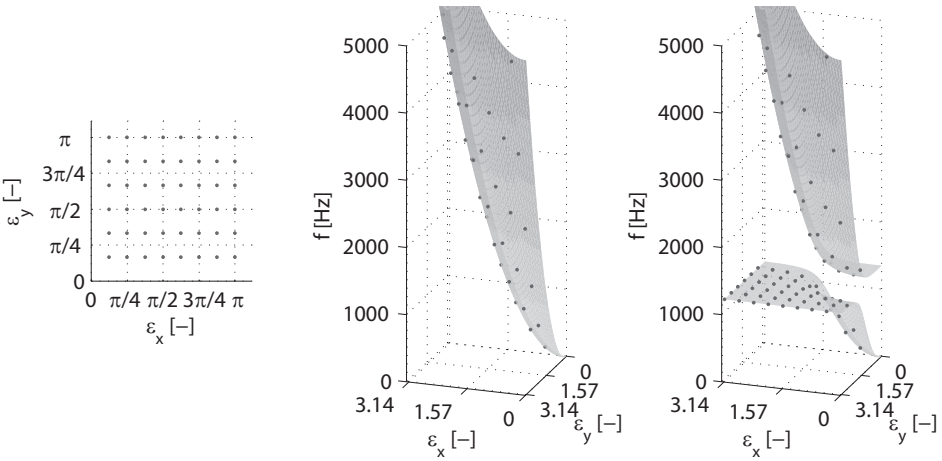

Figure 4: Comparison between the dispersion surfaces of an infinite periodic structure and the eigenmodes (dark bullets (•)) of a finite counterpart (8 x 6 repetitions of the unit cell). Center: a steel plate. Right: a steel plate with a periodic grid of TRs, tuned at half the coincidence frequency of the original plate. Left: locations of the eigenfrequencies in the wave domain.

Figure 4 show the dispersion surfaces for the cases with and without resonators. The eigenfrequencies of the finite plates are indicated with dark bullets (•). It is clear that reducing the infinite structure to a finite structure, corresponds to a sampling of the dispersion surfaces on a rectangular grid as indicated by Mead and Parthan [17]. This means that no modes within a stop

band will be found since this corresponds to a frequency zone where no dispersion surface passes through. This also means that the dispersion curves of previous section, indicating the limits of the dispersion surfaces, are a useful tool for evaluating both finite and infinite structures.

From figure 4 it can be seen that the additional dispersion surface, created by the addition of TRs, results in $N_x \times N_y$ additional modes. This is expected since $N_x \times N_y$ degrees of freedom are added to the system.

4.2. Interpretation of dispersion surface split

More insight into the split of dispersion surfaces is gained by comparing the eigenmodes of the plate without TRs to the plate with TRs. As a comparison tool, a Modal Assurance Criterion (MAC) is used [18]. The MAC indicates the degree of consistency between mode shapes without taking the frequency difference into account. A MAC value of 1 indicates that two modes are consistent, while a MAC value of 0 indicates a lack of consistency between those modes. The MAC is calculated based on all dofs of all the nodes of the plate without TRs.

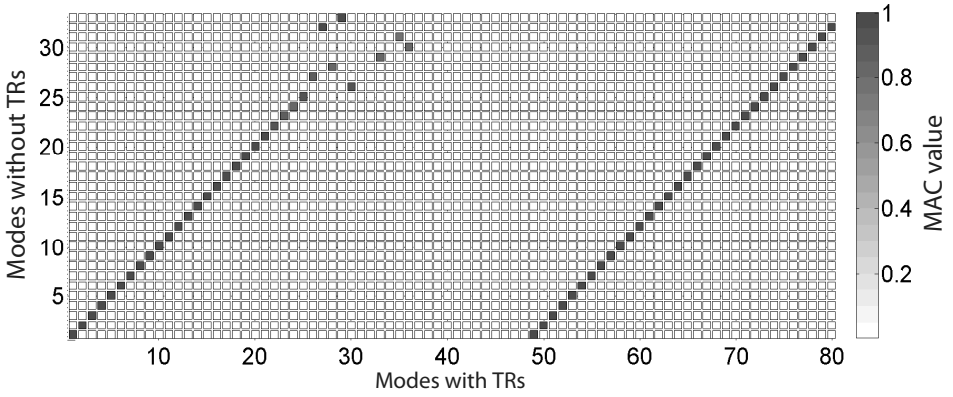

Figure 5: MAC for a finite plate without TRs (vertical axis) and a plate with TRs tuned at half the coincidence frequency of the plate (horizontal axis). Modes up to 5000 Hz are taken into account. The relationship between mode numbers and frequencies are given in Table 3 and Table 4

Figure 5 shows the MAC matrix, which should be interpreted with the help of Table 3 and Table 4. In the case of the plate with a periodic grid of TRs, the first 48 modes correspond to in-phase motion of the plate and the TRs; the following modes correspond to out-of-phase motion

Table 3: Mode numbers and frequencies (Hz) for plate with TRs (horizontal axis in Fig. 5)

1	2	3	4	5	6	7	8	9	10
193,5	398,9	554,7	720,2	737,8	979,9	1015,0	1037,8	1088,9	1134,1
11	12	13	14	15	16	17	18	19	20
1151,8	1165,5	1178,8	1186,9	1187,5	1188,7	1199,4	1199,9	1204,4	1206,5
21	22	23	24	25	26	27	28	29	30
1208,0	1208,0	1210,3	1211,1	1213,1	1213,2	1213,6	1213,9	1214,0	1214,0
31	32	33	34	35	36	37	38	39	40
1214,9	1215,9	1216,1	1216,5	1217,1	1217,7	1218,3	1218,3	1218,6	1219,7
41	42	43	44	45	46	47	48	49	50
1219,9	1220,3	1220,4	1221,2	1221,4	1221,7	1222,0	1222,2	1352,1	1362,5
51	52	53	54	55	56	57	58	59	60
1378,0	1407,6	1412,1	1536,4	1576,2	1609,5	1719,1	1900,0	2020,0	2154,2
61	62	63	64	65	66	67	68	69	70
2343,4	2497,0	2515,1	2547,5	2894,7	2943,3	3139,6	3313,7	3388,7	3512,2
71	72	73	74	75	76	77	78	79	80
3719,2	3903,3	3937,6	4029,8	4065,7	4270,3	4552,6	4816,4	4884,4	4997,3

of the plate and the TRs. A good correlation is found between the modes of the plate without TRs and for both the in phase and out of phase modes of the plate with TRs. The addition of local resonators creates a duplication of the original eigenfrequencies; one set of eigenfrequencies corresponds to in phase motion of the TRs and the plate, the other set of eigenfrequencies corresponds to out of phase motion of the TRs and the plate.

A good correlation is found between the modes of the plate without TRs and both the in-phase and out-of-phase modes of the plate with TRs. When inspecting modes close to the resonance frequency of the TRs high amplitudes are found in the point masses of the TRs and low amplitudes in the plate itself. These modes correspond with the modes on the flat parts on the dispersion surfaces on figure 4 (graph on the right), or the modes with mode number 10 to 50 in

Table 4: Mode numbers and frequencies (Hz) for plate without TRs (vertical axis in Fig. 5)

1	2	3	4	5	6	7	8	9	10
212,9	442,3	622,1	825,1	847,9	1225,6	1302,5	1359,9	1524,1	1754,5
11	12	13	14	15	16	17	18	19	20
1894,5	2045,2	2250,7	2413,8	2433,0	2467,2	2828,8	2879,2	3080,8	3259,3
21	22	23	24	25	26	27	28	29	30
3335,7	3462,0	3672,5	3859,5	3893,8	3987,2	4023,7	4230,9	4515,8	4781,9
31	32	33							
4850,5	4930,7	4983,4							

Table 3. Although the amplitude in the plate itself is low for these modes, the vibrational pattern in the plate itself still shows a relative high correlation with the modes of the plate without TRs.

Especially the modes right after the stop band correlate well (MAC value >0.95) with the low-frequency modes of the original plate. This means that the originally low frequency vibration pattern of the plate without TRs are repeated at a higher frequency for the plate with TRs. This results in originally not efficiently radiating vibration patterns, corresponding to long wave lengths, to be copied at higher frequencies, making them efficiently radiating. In eq. (3) this corresponds to a rise in the frequency of propagation f for the same structural wave length k_{str} resulting in an out-of-plane component $k_{\perp}$ of the acoustic wave that becomes propagating.

5. Application on a finite steel plate

To assess the importance of the changes in radiation efficiency for practical applications, the finite counterparts of the infinite plates are investigated acoustically. A finite plate is derived from the unit cell model in accordance with previous section. The plate is excited in the out-of-plane direction at the point with coordinates (0.117;0.108) in a coordinate system according to Fig. 3 (origin in the bottom left corner of the plate). The excited node is marked with a light sphere. The TRs have 1% of critical damping (viscous) and the plate is 1% structurally damped by adding a complex part to the E-modulus of Table 1. For a discussion of the effect of damping,

the interested reader is referred to previous work [4].

Four cases are compared: the plate with TRs tuned at 50, 100 and 160% of the coincidence frequency of the original plate and the equivalent plate. All plates have the same weight since this is an important factor for acoustic behaviour.

To derive the acoustic radiation, the structural FEM is coupled to an acoustic FEM surrounding the structure with an Automatically Matched Layer property on the free boundary. LMS VL.Acoustics software was used to solve this problem in a direct vibro-acoustic coupled way. A direct solver was chosen to be able to take localized damping in the tuned resonators into account. The acoustic mesh is built with 171834 nodes and 54748 linear Tetra4 elements. Convergence of both the structural and acoustic model was checked.

The radiation efficiency σ allows evaluation of the acoustic coupling between the structural and the acoustic domain:

$$\sigma = \frac{W}{2\rho c_{ac} v_{CRSS}^2}, \tag{6}$$

$$v_{CRSS} = \sqrt{\int_S Re(vv^*) dS}, \tag{7}$$

with W the radiated acoustic power, ρ the density of air, c_{ac} the speed of sound in air, S the wetted surface of the plate and v the velocity on a point of the plate, $\bullet^*$ denotes the complex conjugate of $\bullet$. The factor 2 in the denominator of eq. (6) compensates for the integration in eq. (7) across one side of the plate while the plate radiates acoustically to 2 sides. Equation (7) expresses the continuous averaged root mean square sum (CRSS) of the plate vibration averaged across the plate. The integral in eq. (7) is evaluated by taking a weighted sum of the velocities at the nodes in the structural modal. The weights in the weighted sum express the part of the surface that each node represents.

Figure 6 compares the radiation efficiency, the radiated acoustic power and the CRSS displacements of the plate for the different test cases. This should be analyzed together with Fig. 2 and Table 2. The equivalent plate serves as a benchmark for comparison with the plates showing stop band behaviour. The predicted stop bands correspond to zones of reduced vibration which

manifests itself as well in the radiated acoustic power.

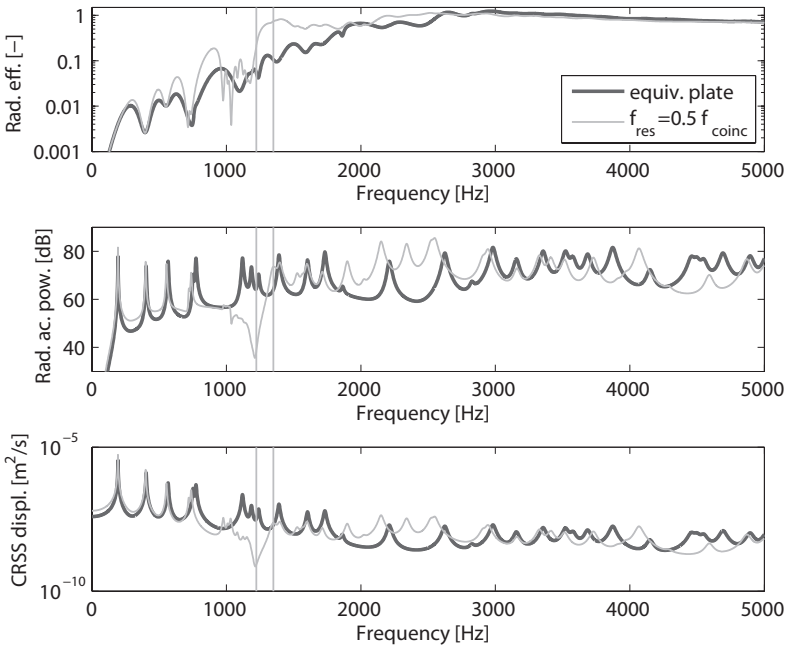

Figure 6: Radiation efficiency, radiated acoustic power and CRSS displacements. The thin light line (—) represents a plate with a grid of TRs tuned at 0.5 times the coincidence frequency of the steel plate without TRs. The vertical lines indicate the stop band zones according to table 2. The dark line (—) represents a finite steel plate with an increased density to match the weight of the TRs.

TRs tuned at half the coincidence frequency (Fig. 6) lead to an increase in radiation efficiency in a zone above the stop band; despite the lower vibration levels in this frequency zone, the acoustic radiated power is matching the levels of the equivalent plate. This is especially of importance since local resonance based stop bands are often characterized by a zone of increased vibrations for frequencies just above the stop band frequencies [4].

TRs tuned at the coincidence frequency of the original plate (Fig. 7) show both good vibrational and acoustic behaviour. Also TRs tuned at a frequency 160% of the coincidence frequency (Fig. 8) show both a good vibrational and acoustic response. The extra zone of efficient acous-

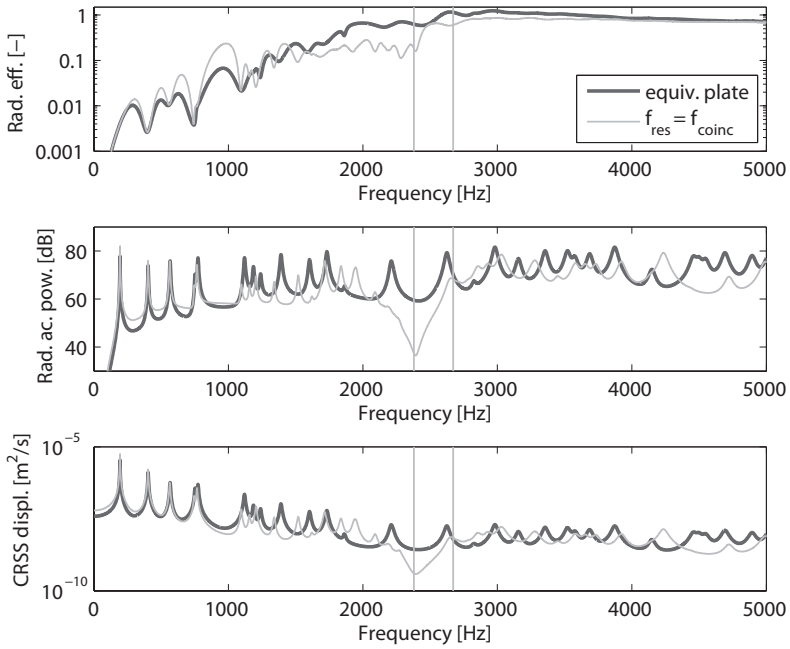

Figure 7: Radiation efficiency, radiated acoustic power and CRSS displacements. The thin light line (—) represents a plate with a grid of TRs tuned at the coincidence frequency of the steel plate without TRs. The vertical lines indicate the stop band zones according to table 2. The dark line (—) represents a finite steel plate with an increased density to match the weight of the TRs.

tic radiation, Table 2, is not strongly pronounced in comparison with the equivalent plate since the equivalent plate is also efficiently radiating in this frequency zone. For both cases, the radiation efficiency of the plate with TRs is clearly improved in comparison with the equivalent plate.

The coincidence frequency is in general used as a measure to decide between efficient radiation or not. Below coincidence the radiation efficiency will gradually increase with frequency until coincidence is reached. This increase in radiation efficiency is linked to the gradual decrease in difference between the structural wave vector magnitude and the acoustic wave vector magnitude.

Figures 9 to 11 underline this by comparing the radiation efficiency for the cases of Fig. 6 to 8

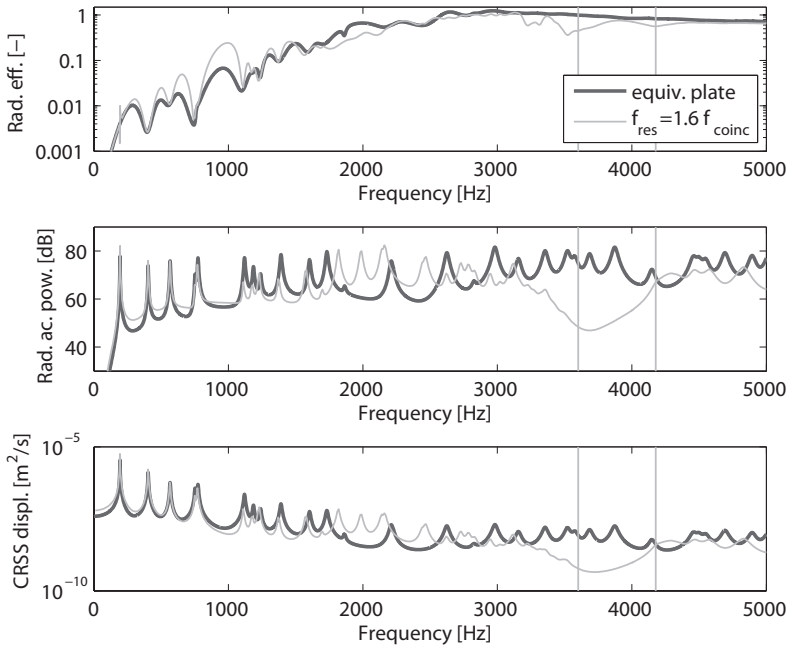

Figure 8: Radiation efficiency, radiated acoustic power and CRSS displacements. The thin light line (—) represents a plate with a grid of TRs tuned at 1.6 times the coincidence frequency of the steel plate without TRs. The vertical lines indicate the stop band zones according to table 2. The dark line (—) represents a finite steel plate with an increased density to match the weight of the TRs.

with the difference in structural and acoustic wave vector magnitude as function of frequency. The acoustic wave magnitude is expressed as propagation vector magnitude, i.e. phase shift per unit cell $\|k_{ac}.L_{UC}\|$ in order to compare this to the structural propagation vector magnitude $\|\vec{\epsilon}\|$ of the propagation vectors on the Brillouin contour (Fig. 2); the difference in wave magnitudes in Fig. 9 to 11 thus relates to the distance between the dispersion curves of the structure and air for a given frequency in Fig. 2; a negative difference indicates efficient radiation.

Closer inspection gives further insight in the difference in radiation efficiency between the plate with TRs and the plate with an equivalent mass.

- The zone of inefficient radiation (positive difference in wave vector magnitude) between the two coincidence regions for the case of TRs tuned at half the coincidence frequency,

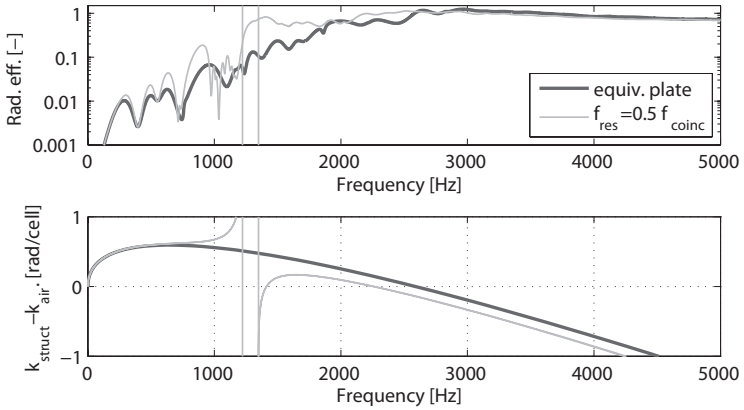

Figure 9: Radiation efficiency and difference between structural and acoustical wave vector magnitude. The thin light line (—) represents a plate with a grid of TRs tuned at 0.5 the coincidence frequency of the steel plate without TRs. The vertical lines indicate the stop band zones according to table 2. The dark line (—) represents a finite steel plate with an increased density to match the weight of the TRs.

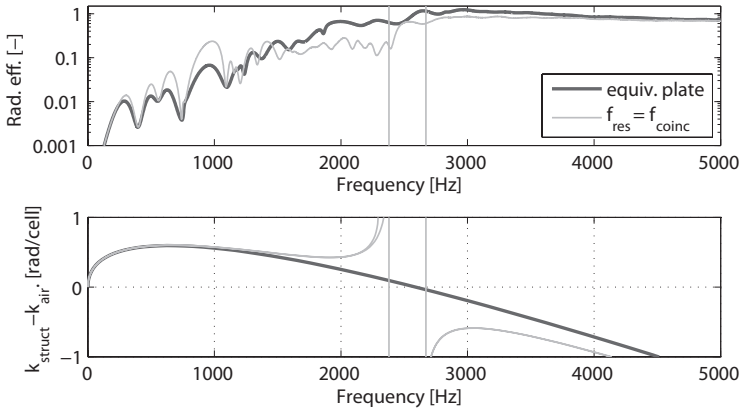

Figure 10: Radiation efficiency and difference between structural and acoustical wave vector magnitude. The thin light line (—) represents a plate with a grid of TRs tuned at the coincidence frequency of the steel plate without TRs. The vertical lines indicate the stop band zones according to table 2. The dark line (—) represents a finite steel plate with an increased density to match the weight of the TRs.

Table 2, seems to be still more efficient as the inefficient radiation of the equivalent plate. From Fig. 9 it is clear that in this zone, the structural and acoustic wave are a closer match than for the plate with an equivalent weight.

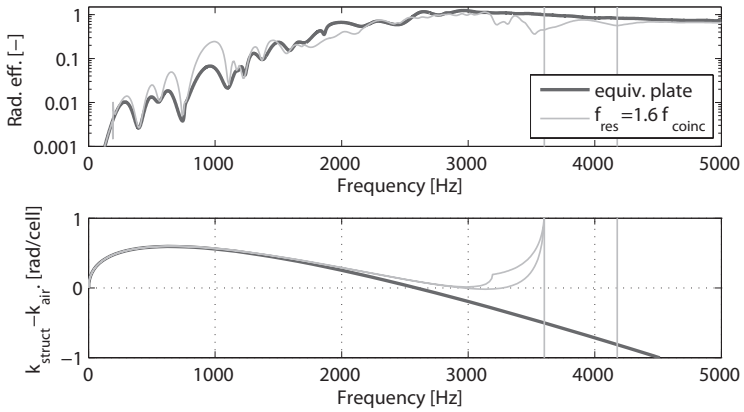

Figure 11: Radiation efficiency and difference between structural and acoustical wave vector magnitude. The thin light line (—) represents a plate with a grid of TRs tuned at 1.6 times the coincidence frequency of the steel plate without TRs. The vertical lines indicate the stop band zones according to table 2. The dark line (—) represents a finite steel plate with an increased density to match the weight of the TRs.

- For the case of TRs tuned at the coincidence frequencies it can be seen that the radiation efficiency before the stop band is lower for the plate with TRs as for the equivalent plate although both are not yet efficiently radiating. In this case the difference in structural wave vector and acoustic wave vector is increased before the stop band due to the added TRs, leading to a decrease in radiation efficiency.

- In the case of TRs tuned at 160% of the coincidence frequency the same effects manifest themselves, due to the dispersion curve of the structure bending away from the dispersion curve of air before the stop band, a zone of less efficient radiation is created in comparison with the already efficiently radiating equivalent plate. A zone of decreased radiation efficiency is the result.

6. Conclusions

The potential of stop bands to improve the vibrational behavior of structures is shown in literature. This paper investigates the acoustic radiation efficiency of local resonance based stop band materials both for infinite structures as well as their finite counterpart. Based on the addition of a

grid of tuned resonators, it is shown that care should be taken in designing stop bands for vibro-acoustic applications since the characteristic mode split in resonance based stop band materials can drastically influence the radiation efficiency of those materials. A stop band designed below the coincidence frequency of the original structure creates an additional zone of increased radiation efficiency for a frequency zone just above the stop band region. A stop band applied at or above the coincidence frequency reduces the total zone of efficient acoustic radiation. In this last case, the beneficial vibrational effect of a stop band is acoustically enforced.

To obtain good acoustic stop band behaviour, general practice should be to design TRs above coincidence. In view of low frequent solutions, stop bands are thus more promising in application such as composites and lightweight structures which are in general characterised by lower coincidence frequencies.

7. Acknowledgements

The research of Claus Claeys is funded by a Ph.D. grant of the Institute for the Promotion of Innovation through Science and Technology in Flanders (IWT-Vlaanderen). The IWT Flanders within the ASTRA project and the European Commission within the FP7 eLiQuiD Marie Curie European Industry Doctorate (GA 316422) and the ITN Marie Curie project GA-290050 GRESIMO are also gratefully acknowledged for their support.

References

[1] Z. Liu, X. Zhang, Y. Mao, Y. Zhu, Z. Yang, C. Chan, P. Sheng, Locally resonant sonic materials, Science 289 (2000) 1734–1736.

[2] Y. Xiao, J. Wen, D. Yu, X. Wen, Flexural wave propagation in beams with periodically attached vibration absorbers: Band-gap behavior and band formation mechanisms, Journal of Sound and Vibration 332 (2012) 867–893.

[3] P. Sheng, C. Chan, Classic wave localization and spectral gap materials, International Journal for structural, physical and chemical aspects of crystalline material 220 (2005) 757–764.

[4] C. Claeys, K. Vergote, P. Sas, W. Desmet, On the potential of tuned resonators to obtain low-frequency vibrational stop bands in periodic panels, Journal of Sound and Vibration 332 (2012) 1418–1436.

[5] D. Mead, Free wave propagation in periodically supported, infinite beams, Journal of Sound and Vibration 11 (1970).

[6] D. J. Mead, Plates with regular stiffening in acoustic media: Vibration and radiation, The Journal of the Acoustical Society of America 88 (1990).

[7] F. Casadei, L. Dozio, M. Ruzzene, K. Cunefare, Periodic shunted arrays for the control of noise radiation in an enclosure, Journal of Sound and Vibration 329 (2010) 3632–3646.

[8] M. Collet, M. Ouisse, M. Ichchou, R. Ohayon, Semi-active optimization of 2d wave dispersion into shunted piezo-composite systems for controlling acoustic interaction, Smart Materials and Structures 21 (2012) 094002.

[9] M. Strasberg, D. Feit, Vibration damping of large structures induced by attached small resonant structures, The Journal of the Acoustical Society of America 99 (1996) 335.

[10] M. Jolly, J. Sin, Passive tuned vibration absorbers for sound radiation reduction from vibrating panels, Journal of sound and vibration 191 (1996) 577–583.

[11] L. Brillouin, Wave propagation in periodic structures, McGraw-Hill Book Company, New York, 1946.

[12] C. Kittel, Introduction to Solid State Physics, volume 119 of [15], 8 edition, 2005.

[13] A. R. Diaz, A. G. Haddow, L. Ma, Design of band-gap grid structures, Structural and Multidisciplinary Optimization 29 (2005) 418–431.

[14] R. Langley, A note on the force boundary conditions for two-dimensional periodic structures with corner freedoms, Journal of Sound and Vibration 167 (1993) 377–381.

[15] A. Srikantha Phani, J. Woodhouse, N. A. Fleck, Wave propagation in two-dimensional periodic lattices, The Journal of the Acoustical Society of America 119 (2006) 1995–2005.

[16] F. Fahy, Sound and structural vibration: radiation, transmission and response, Academic Pr, 1987.

[17] D. Mead, S. Parthan, Free wave propagation in two-dimensional periodic plates, Journal of Sound and Vibration 64 (1979) 325–348.

[18] R. J. Allemang, The modal assurance criterion–twenty years of use and abuse, Sound and Vibration 37 (2003) 14–23.

[19] S. Cox, D. Dobson, Maximizing band gaps in two-dimensional photonic crystals, SIAM Journal on Applied Mathematics 59 (1999) 2108–2120.

[20] X. Liu, G. Hu, C. Sun, G. Huang, Wave propagation characterization and design of two-dimensional elastic chiral metacomposite, Journal of Sound and Vibration 330 (2011) 2536–2553.

List of Figures

List of Tables